



HAL
open science

Low Temperature Kinetics of the First Steps of Water Cluster Formation

Jérémy Bourgalais, V. Roussel, Michael Capron, Abdessamad Benidar, A. W. Jasper, S. J. Klippenstein, Ludovic Biennier, Sébastien D. Le Picard

► **To cite this version:**

Jérémy Bourgalais, V. Roussel, Michael Capron, Abdessamad Benidar, A. W. Jasper, et al.. Low Temperature Kinetics of the First Steps of Water Cluster Formation. *Physical Review Letters*, 2016, 116 (11), pp.113401. 10.1103/PhysRevLett.116.113401 . hal-01301357

HAL Id: hal-01301357

<https://hal-univ-rennes1.archives-ouvertes.fr/hal-01301357>

Submitted on 10 Nov 2022

HAL is a multi-disciplinary open access archive for the deposit and dissemination of scientific research documents, whether they are published or not. The documents may come from teaching and research institutions in France or abroad, or from public or private research centers.

L'archive ouverte pluridisciplinaire **HAL**, est destinée au dépôt et à la diffusion de documents scientifiques de niveau recherche, publiés ou non, émanant des établissements d'enseignement et de recherche français ou étrangers, des laboratoires publics ou privés.

Low Temperature Kinetics of the First Steps of Water Cluster Formation

J. Bourgalais,¹ V. Roussel,¹ M. Capron,^{1,*} A. Benidar,¹ A. W. Jasper,² S. J. Klippenstein,^{3,†}
L. Biennier,¹ and S. D. Le Picard^{1,‡}

¹*Institut de Physique de Rennes, UMR 6251 CNRS-Université de Rennes 1,
263 avenue Général Leclerc, 35042 Rennes cedex, France*

²*Combustion Research Facility, Sandia National Laboratories, Livermore, California 94551, USA*

³*Chemistry Division, Argonne National Laboratory, Argonne, Illinois 60439, USA*

(Received 27 July 2015; published 17 March 2016)

We present a combined experimental and theoretical low temperature kinetic study of water cluster formation. Water cluster growth takes place in low temperature (23–69 K) supersonic flows. The observed kinetics of formation of water clusters are reproduced with a kinetic model based on theoretical predictions for the first steps of clusterization. The temperature- and pressure-dependent association and dissociation rate coefficients are predicted with an *ab initio* transition state theory based master equation approach over a wide range of temperatures (20–100 K) and pressures (10^{-6} – 10 bar).

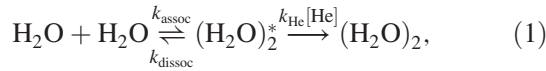
DOI: 10.1103/PhysRevLett.116.113401

Nucleation phenomena are of interest for a large variety of scientific fields from physics, chemistry, or biology to nanotechnology, atmospheric sciences, or medicine. Although nucleation processes have been intensively studied for more than two centuries (see Ref. [1] and references therein), major uncertainties remain in our understanding of the mechanisms for particle formation. A number of experimental methods have been developed for achieving supersaturation conditions at various temperatures using mainly adiabatic expansions, diffusion chambers, or laminar flow tube reactors (see Ref. [2] and references therein). These methods generally provide a means for estimating the nucleation rates, i.e., the number of nuclei formed per unit time and per unit volume, as a function of saturation and temperature. These rates vary over orders of magnitude as they appear to be very sensitive to the physical conditions, such as the temperature of the environment or the concentrations and the nature of the species involved. Classical nucleation theory, which has long been the most commonly used theoretical method for describing nucleation processes, fails to provide accurate estimates of the absolute nucleation rates [3–5]. This shortcoming motivates continuing efforts to develop a fundamental understanding of the nucleation mechanisms at the molecular level where the intermolecular interaction potential is of crucial importance. Fifteen years ago, Garrett and co-workers [6] proposed a new theoretical approach for modeling vapor-phase nucleation in which the evaporation and condensation processes are treated as gas-phase dissociation and association reactions. In this approach, variational transition state theory is used to directly calculate dissociation and association rate coefficients [6]. Such a dynamical treatment requires an accurate description of the intermolecular potential, the reaction rates being very sensitive to the details of the molecular interactions.

Of particular interest is the nucleation of water. Water is involved in various natural nucleation processes, such as the formation of droplets and particles in the atmosphere [7], which are still poorly understood [2]. Even though it is unclear whether water vapor ever nucleates itself in Earth's atmosphere, its homogeneous nucleation has served as a valuable prototype for understanding the formation of clusters at the molecular level [3,8–11]. Several experimental devices have been used to study homogeneous condensation of neutral water vapor [12–14], delivering nucleation rates in different saturation and temperature conditions. Comparison with experiments realized under different and well-controlled conditions is of major importance for testing and improving the theoretical models, as nucleation rates can vary over orders of magnitude. Such comparisons generally focus on the critical cluster formation rate, which requires an accurate prediction of the critical cluster formation free energy. At the molecular level, nucleation is usually considered as a multistep process building from successive monomer addition reactions, and prediction of absolute nucleation rates requires accurate rates for each of the elementary reaction steps.

In this Letter, we report an experimental and theoretical kinetic study of neutral water cluster formation at low temperature. The experiments are performed using cold uniform supersonic flows of helium generated by a series of Laval nozzles in a CRESU (Cinétique de Réaction en Ecoulement Supersonique Uniforme) apparatus [15], in which a small (< 1%) and controlled amount of water vapor is introduced. At the low temperatures of the present experiments, the dissociation rates are so low that evaporation can be neglected. The kinetics then corresponds to a barrierless process that is governed by the kinetics of collisions, with dimer formation being the critical step [16]. A kinetic model based on theoretical predictions of the rate

coefficients for the first steps of clusterization is used to fit the observed kinetics of formation of water clusters. The formation of water clusters can be treated in terms of bimolecular formation of energized clusters, which can then either be stabilized by collision with a third body (helium here) or redissociate. For instance, within the Rice-Ramsperger–Kassel–Marcus theory the dimer formation from two monomers can be treated as follows:



where k_{assoc} and k_{dissoc} are the association and dissociation rate coefficients, respectively, and k_{He} is the rate coefficient for deactivation of the energized complexes, $(\text{H}_2\text{O})_2^*$, by collisions with the helium buffer gas.

Four Laval nozzles (Table S1 of Supplemental Material [17]) are used in this study to generate supersonic flows at well-defined temperatures (from 22.9 to 69.4 K), with various total densities (from 4.75 to 10.45×10^{16} molecule cm^{-3}). In order to monitor the time evolution of neutral monomers as well as clusters formed in these flows, an ionization mass spectrometry technique is used after skimming out the center of the flows at various distances from the Laval nozzle exits. Larger distances correlate with longer cluster formation times within the supersonic flow. A similar experimental setup was previously used by Sabbah *et al.* to study pyrene dimer formation [37]. Here, instead of single photon ionization, a 70 eV electron gun is implemented to ionize the neutral water monomers and clusters. Cations formed are then accelerated and guided to reach the extraction zone of a linear time-of-flight mass spectrometer. A schematic diagram of the experimental setup is provided in Fig. S1 of Supplemental Material [17].

The ion mass spectra obtained after electron impact ionization images the distribution of neutral water monomers and clusters. Figure 1 shows the ion signals recorded by the time-of-flight mass spectrometer as a function of the mass-to-charge ratio m/z . These mass spectra are obtained after electron impact ionization for two different initial water monomer densities, hereafter $[\text{H}_2\text{O}]_0$, introduced in the flow generated by the Laval nozzle working at 22.9 K. The exit of the Laval nozzle is set here at 11 cm from the skimmer, which corresponds to 66 μs . For the lowest water monomer density introduced in the flow, $[\text{H}_2\text{O}]_0 = 13 \times 10^{13}$ cm^{-3} , only the H_2O^+ ion signal at a mass-to-charge ratio m/z of 18 can be observed (upper panel). For larger $[\text{H}_2\text{O}]_0$, a distribution of protonated water clusters, $\text{H}^+(\text{H}_2\text{O})_{n-1}$, appears. To derive the distribution of the neutral water monomers and clusters from the mass spectra, the effect of electron impact ionization has to be considered. Electron impact ionization of neutral water clusters is well known to quickly form energetically excited protonated species [38]. Their excess internal energy is dissipated via the evaporation of water monomers. The first water monomer evaporation from the protonated cluster is expected to take place within a few microseconds and should

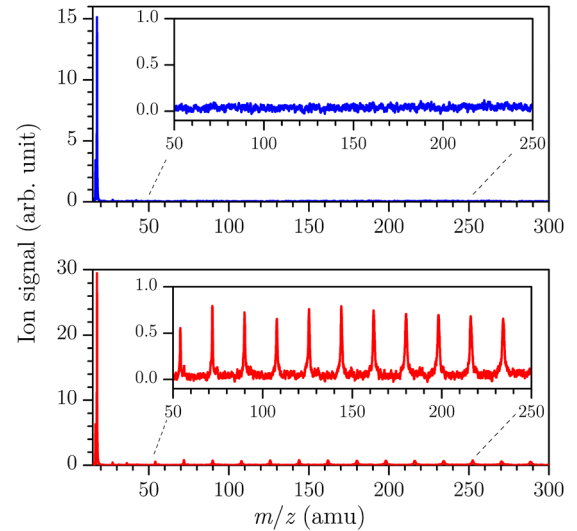


FIG. 1. Mass spectra of protonated water monomers and clusters imaging the neutral water monomers and clusters formed in the supersonic flow at 22.9 K recorded 66 μs after exit from the Laval nozzle. Upper panel: $[\text{H}_2\text{O}]_0 = 13 \times 10^{13}$ cm^{-3} . Lower panel: $[\text{H}_2\text{O}]_0 = 40 \times 10^{13}$ cm^{-3} . In both panels, the inset displays magnification of the ion signals.

be faster for bigger clusters [39–41]. As the loss of a second water monomer should occur tens of microseconds later [40,41], we assume that, for our experimental conditions, every protonated cluster undergoes only one evaporation (see Supplemental Material [17]). Protonated clusters of size n detected by the time-of-flight mass spectrometer after ionization originate, therefore, from neutral clusters of size $n + 2$ formed in the supersonic flows. It is worth noting, however, that evaporation from the smallest clusters is known to be less efficient [40,41]. Furthermore, they take less time than bigger clusters to reach the time-of-flight mass spectrometer. Thus, the smallest protonated clusters detected by the mass spectrometer are likely to originate from neutral clusters of both size $n + 1$ and $n + 2$.

Our experiments allow us to follow the time dependence of ion water monomer and cluster signals providing an image of the neutral clusterization process for various initial neutral water monomer densities, and for all temperature and density conditions generated by the Laval nozzles used here. An absolute measurement of $[\text{H}_2\text{O}](t)$ can be derived from the ion monomer signal when only water monomers are present in the flow, since the density of water introduced in the supersonic flow is known. Figure 2 displays the temporal evolution of $[\text{H}_2\text{O}]$ for the two initial densities of water vapor used to record the spectra shown in Fig. 1 at 22.9 K. It can be seen that the water monomer density remains constant for the lower initial density introduced in the flow, while for the larger initial water vapor density, it decreases with time due to the gradual formation of larger clusters in the flow. The maximum time shown in Fig. 2, 100 μs , correlates with the total length of this supersonic flow (Table S1 of Ref. [17]).

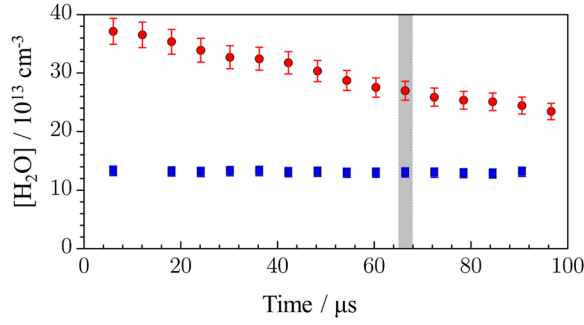


FIG. 2. Time evolution of $[\text{H}_2\text{O}]$ in the supersonic flow at 22.9 K for $[\text{H}_2\text{O}]_0$ of $13 \times 10^{13} \text{ cm}^{-3}$ (blue square) and $40 \times 10^{13} \text{ cm}^{-3}$ (red circle). Error bars combine a small statistical contribution minimized by averaging 65 000 acquisitions of the ion signal and a larger systematic contribution arising from the fluctuations of water flow rate, chamber pressure, and ion transmission. The gray area highlights the time ($66 \mu\text{s}$) at which the mass spectra displayed in Fig. 1 were recorded.

For water clusters, the integrated ion signals $I_n(t)$ depend on their ionization cross sections, and the transmission and detection efficiencies of the experimental setup, all of which are size dependent and not readily accessible experimentally. Thus, they do not directly yield cluster populations, and we instead presume they are related through the expression $I_n = \gamma_{n+2} [(\text{H}_2\text{O})_{n+2}]$, where γ_{n+2} is a size-dependent proportionality factor. Figure 3 shows the temporal evolution on a relative scale of neutral water clusters derived from the ion signals for various cluster sizes at 35.9 K.

A theory informed kinetic model for water cluster formation has been developed and its predictions are compared below with the experimentally observed time evolution of the cluster distributions. In the model [Eqs. (2) and (3)] we assume that a cluster of n molecules can be formed by the addition of two clusters or a cluster and a monomer and that any cluster loss is due to reaction with another cluster or a monomer. Dissociation from the clusters is ignored due to the low temperatures of the present experiments (Table S4 of Ref. [17]). For the association between $(\text{H}_2\text{O})_i$ and $(\text{H}_2\text{O})_j$, with i and j both greater than unity, the evaporation of a monomer from the initially formed adduct is significantly exothermic. As a result, at least for the specific systems examined theoretically, such association processes lead to the evaporation of a monomer with a rate coefficient equal to the high pressure association rate. The stabilization rate is effectively zero. For very large clusters, stabilization of the $i+j$ adduct may ultimately become competitive with monomer evaporation from that adduct, but that effect is ignored here. In summary, the present model is described by the following scheme:

$$\frac{d[\text{H}_2\text{O}]}{dt} = - \sum_{i=1}^N \alpha_{1,i} k_{1,i} [\text{H}_2\text{O}] [(\text{H}_2\text{O})_i] + \sum_{i=2}^N \sum_{j=2}^N \beta_{i,j} k_{i,j} [(\text{H}_2\text{O})_i] [(\text{H}_2\text{O})_j], \quad (2)$$

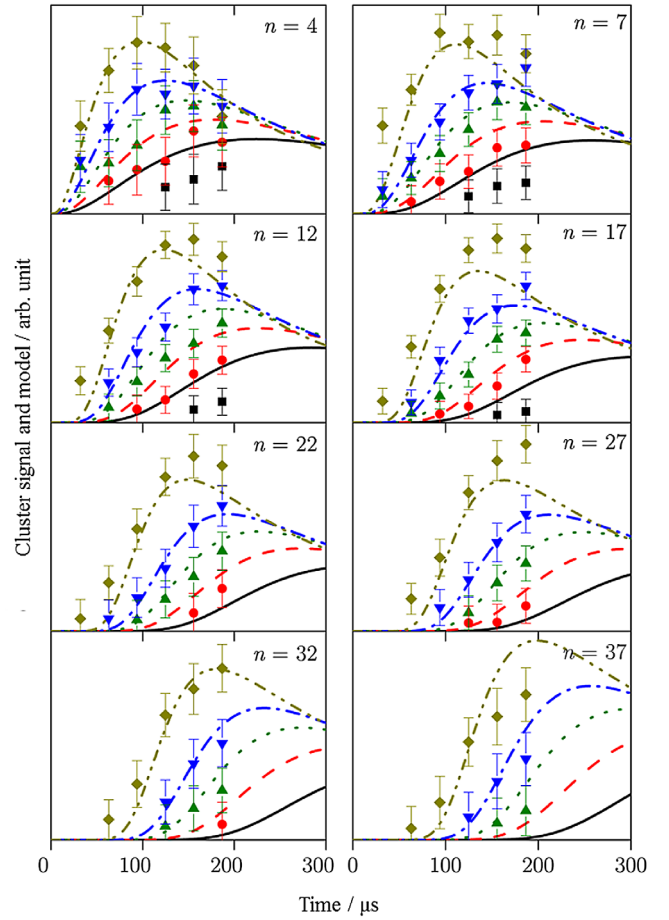


FIG. 3. Time evolution of $(\text{H}_2\text{O})_n$ clusters at 35.9 K for $[\text{H}_2\text{O}]_0$ equals to black square and black solid line, 1.22; red circle and red dashed line, 1.54; dark green triangle and dark green dotted line, 1.85; blue downward triangle and blue dot-dashed line, 2.17; light green lozenge and light green dot-dot-dashed line, 2.79 ($\times 10^{14} \text{ molecule cm}^{-3}$). Lines refer to the kinetic model with calculated rate constants of Table S2 [17].

$$\begin{aligned} \frac{d[(\text{H}_2\text{O})_n]}{dt} = & + \alpha_{1,n-1} k_{1,n-1} [\text{H}_2\text{O}] [(\text{H}_2\text{O})_{n-1}] \\ & - \sum_{i=1}^N \alpha_{n,i} k_{n,i} [(\text{H}_2\text{O})_n] [(\text{H}_2\text{O})_i] \\ & + \sum_{i=1}^{n-2} \beta_{i+1,n-i} k_{i+1,n-i} [(\text{H}_2\text{O})_{i+1}] [(\text{H}_2\text{O})_{n-i}], \end{aligned} \quad (3)$$

where N is the largest cluster size considered in the calculations; $\alpha_{i,j}$ is a stoichiometric coefficient: $\alpha_{i,j} = 2$ for $i = j$ and $\alpha_{i,j} = 1$ for $i \neq j$; and $\beta_{i,j}$ corrects for double counting: $\beta_{i,j} = 1$ for $i = j$ and $\beta_{i,j} = 0.5$ for $i \neq j$ and $n \geq 2$.

Temperature- and pressure-dependent association rate coefficients, $k_{i,j}(T, P)$, were predicted with an *ab initio* transition state theory based master equation approach for $(i, j) = (1, 1), (1, 2), (1, 3), (1, 4), (1, 5), (2, 2), (2, 3), (2, 4),$ and $(3, 3)$. This approach couples transition state theory based evaluations of the microcanonical dissociation rate

coefficients, $k_{\text{dissoc}}(E)$, with simple models for collision-induced energy transfer rates, $k_c(E \rightarrow E')$, to obtain a master equation for the time dependence of the energy resolved state populations. The thermal association rate coefficient, $k_{i,j}(T, P)$, is then obtained from the eigensolutions of this master equation. *Ab initio* electronic structure theory was used to evaluate the reactant and transition state properties required for the evaluation of $k_{\text{dissoc}}(E)$ and the molecular partition functions. The transition state partition functions are evaluated with variable reaction coordinate transition state theory, which accounts for the full anharmonicity and mode coupling in the key reactive modes via Monte Carlo evaluation of configurational integrals. This approach requires potential energy values for the interaction between rigid reactants at arbitrary separations and orientations, which are obtained here via direct *ab initio* evaluations.

The predicted pressure dependence of the rate coefficients for the $\text{H}_2\text{O} + \text{H}_2\text{O}$ and $\text{H}_2\text{O} + (\text{H}_2\text{O})_2$ reactions is illustrated in Fig. 4 for the experimentally studied temperatures. The dissociation energy D_0 is a key parameter in this analysis. For the (1,1) case, we employ the experimental D_0 value of 1105 cm^{-1} [42], within a few cm^{-1} of high-level theoretical values [43,44]. For the (1,2) case, we employ the theoretical D_0 value of 2726 cm^{-1} [45], which is in good agreement with the experimental value of $2650 \pm 50 \text{ cm}^{-1}$ [46]. For the monomer + monomer reaction, the falloff from the high pressure limit is about a factor of 10^{-3} for the experimentally studied pressures. The $k_{1,2}$ rate coefficient approaches its high pressure limit at much lower pressures than does $k_{1,1}$. This result is due to the increase in the number of low frequency modes, which yields a decrease in the rate of dissociation at a given energy, and thus an increase in the probability of collisional stabilization at a given pressure. Further increases in size lead to a similar shift toward the high pressure limit, as illustrated in Fig. S10 of Ref. [17]. The temperature dependence of the high pressure limit rate coefficients is illustrated in Fig. S9 [17].

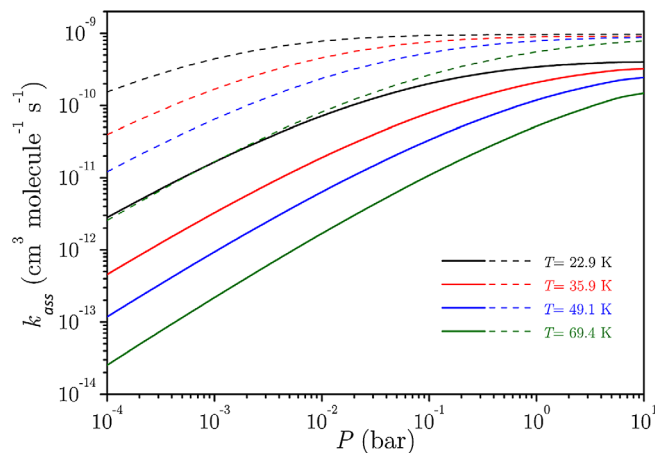


FIG. 4. Theoretically predicted temperature- and pressure-dependent association rate coefficients for $\text{H}_2\text{O} + \text{H}_2\text{O}$ (solid lines) and $\text{H}_2\text{O} + (\text{H}_2\text{O})_2$ (dashed lines). The experimentally studied pressure range is from about 10^{-3} to 10^{-4} bar.

Table S2 [17] presents the calculated association rate coefficients for our experimental conditions. Table S3 [17] provides a more extensive summary of the temperature and pressure dependence of the calculated rate coefficients. It is worth noting that for the present conditions, due to greater pressure falloff the dimer formation rate coefficient is 2 orders of magnitude lower than rates for larger cluster formation. At 22.9 K and 0.165 mbar, for instance, $k_{1,1} = 4.2 \times 10^{-12} \text{ cm}^3 \text{ molecule}^{-1} \text{ s}^{-1}$ and $k_{1,2} = 2.0 \times 10^{-10} \text{ cm}^3 \text{ molecule}^{-1} \text{ s}^{-1}$. This clearly indicates that dimer formation is the rate limiting step for water cluster production in our experimental conditions.

A fitting of the experimental data is undertaken using the kinetic model [Eqs. (2) and (3)] in which the predicted rate coefficients are implemented. For each temperature, values of $k_{i,j}$ for larger i and j are supposed equal to a single rate coefficient k_∞ that is used as a fitting parameter. These fitted k_∞ values, which are also reported in Table S2 [17], are reasonably consistent with the calculated high pressure values for smaller clusters, with some discrepancy observed only for the 69.4 K case, where the data and fitting are more uncertain. Figure 3 shows the comparison between the experimental data and the kinetic model at 35.9 K, for five different initial water densities in the case of neutral clusters composed of 4–37 monomers. As clusters can start to form before the exit of the Laval nozzle because the uniform supersonic flow is already established a few μs upstream, the origin of the time was chosen in the model to fit the experimental measurements. Furthermore, to compare the time evolution given by the model with the experimental data, the population of clusters given by the model was arbitrarily normalized to one of the experimental points. The fit was optimized by minimizing χ^2 using the Nelder-Mead downhill simplex method [47]. The time evolution of the clusters at 22.9, 49.1, and 69.4 K, as well as the results of the fitting procedure, are presented in the Supplemental Material [17]. In addition, a sensitivity study is presented, showing the high influence of the $k_{1,1}$ rate coefficient to the goodness of fit.

The formation of water clusters is a fundamentally interesting physical phenomenon with strong dependence on key parameters such as the temperature and pressure. The present study combines experiments, theoretical calculations, and modeling to directly probe the cluster formation process under low temperature conditions. This study gives access for the first time to quantitative information on the rates of the elementary reactions involved in the first steps of nucleation over a wide range of physical conditions. We demonstrate that at low temperatures, where cluster dissociation is negligible, their growth is controlled by the kinetics of water dimer formation and that this formation is strongly pressure dependent. This control is tighter at low pressure and high temperature, as long as the temperature is not so high that dissociation becomes competitive. Notably, the predicted pressure-dependent falloff in $k_{1,1}$ is even more significant at higher temperature and is also important in the reverse dimer dissociation. This work opens the way to an

investigation of the kinetics of homogeneous nucleation of molecular species. Beyond fundamental aspects, this is of particular interest for the exploration of the condensation processes in cold planetary atmospheres.

The Rennes team acknowledges support from the Agence Nationale de la Recherche, Contract No. ANR-11-BS04-024-CRESUSOL-01, the Institut de Physique (INP-CNRS), the Région Bretagne, and the Université de Rennes 1. S. D. L. P. acknowledges financial support from the Institut Universitaire de France. The Rennes group wishes to express their thanks to Professor P. Casavecchia and Dr. R. Thissen and Dr. E. Hugo for his help in the design of the experiment. This study is based in part on work supported by the U.S. Department of Energy, Office of Science, Office of Basic Energy Sciences, Division of Chemical Sciences, Geosciences, and Biosciences at Argonne under Contract No. DE-AC02-06CH11357, and at Sandia under Contract No. DE-AC04-94AL85000. Sandia is a multiprogram laboratory operated by Sandia Corporation, a Lockheed Martin Company, for the National Nuclear Security Administration.

*michael.capron@univ-rennes1.fr

†sjk@anl.gov

‡sebastien.le-picard@univ-rennes1.fr

- [1] S. M. Kathmann, *Theor. Chem. Acc.* **116**, 169 (2006).
- [2] R. Zhang, A. Khalizov, L. Wang, M. Hu, and W. Xu, *Chem. Rev.* **112**, 1957 (2012).
- [3] J. Merikanto, H. Vehkamäki, and E. Zapadinsky, *J. Chem. Phys.* **121**, 914 (2004).
- [4] J. Merikanto, E. Zapadinsky, A. Lauri, and H. Vehkamäki, *Phys. Rev. Lett.* **98**, 145702 (2007).
- [5] J. Diemand, R. Angélib, K. K. Tanaka, and H. Tanaka, *J. Chem. Phys.* **139**, 074309 (2013).
- [6] G. K. Schenter, S. M. Kathmann, and B. C. Garrett, *Phys. Rev. Lett.* **82**, 3484 (1999).
- [7] G. T. Evans and V. Vaida, *J. Chem. Phys.* **113**, 6652 (2000).
- [8] G. K. Schenter, S. M. Kathmann, and B. C. Garrett, *J. Chem. Phys.* **116**, 4275 (2002).
- [9] S. M. Kathmann, G. K. Schenter, and B. C. Garrett, *J. Chem. Phys.* **116**, 5046 (2002).
- [10] K. K. Tanaka, A. Kawano, and H. Tanaka, *J. Chem. Phys.* **140**, 114302 (2014).
- [11] A. Obeidat, J.-S. Li, and G. Wilemski, *J. Chem. Phys.* **121**, 9510 (2004).
- [12] B. E. Wyslouzil, C. H. Heath, J. L. Cheung, and G. Wilemski, *J. Chem. Phys.* **113**, 7317 (2000).
- [13] V. B. Mikheev, P. M. Irving, N. S. Laulainen, S. E. Barlow, and V. V. Pervukhin, *J. Chem. Phys.* **116**, 10772 (2002).
- [14] A. A. Manka, D. Brus, A.-P. Hyvärinen, H. Lihavainen, J. Wölk, and R. Strey, *J. Chem. Phys.* **132**, 244505 (2010).
- [15] G. Dupeyrat, J. B. Marquette, and B. R. Rowe, *Phys. Fluids* **28**, 1273 (1985).
- [16] H. Vehkamäki and I. Riipinen, *Chem. Soc. Rev.* **41**, 5160 (2012).
- [17] See Supplemental Material at <http://link.aps.org/supplemental/10.1103/PhysRevLett.116.113401>, which includes Refs. [18–36], for details and complementary information on the experimental and theoretical work. All experimental and theoretical data are also presented.
- [18] J. A. Miller and S. J. Klippenstein, *J. Phys. Chem. A* **110**, 10528 (2006).
- [19] S. J. Klippenstein, *J. Chem. Phys.* **96**, 367 (1992).
- [20] S. J. Klippenstein and W. D. Allen, *Ber. Bunsen-Ges. Phys. Chem.* **101**, 423 (1997).
- [21] L. B. Harding, Y. Georgievskii, and S. J. Klippenstein, *J. Phys. Chem. A* **109**, 4646 (2005).
- [22] G. S. Tschumper, B. C. Leininger, B. C. Hoffman, E. F. Valeev, H. F. Schaefer, and M. Quack, *J. Chem. Phys.* **116**, 690 (2002).
- [23] J. R. Lane, *J. Chem. Theory Comput.* **9**, 316 (2013).
- [24] Y. Georgievskii and S. J. Klippenstein, *J. Chem. Phys.* **122**, 194103 (2005).
- [25] S. M. Kathmann, B. J. Palmer, G. K. Schenter, and B. C. Garrett, *J. Chem. Phys.* **128**, 064306 (2008).
- [26] G. K. Schenter, S. M. Kathmann, and B. C. Garrett, *J. Phys. Chem. A* **106**, 1557 (2002).
- [27] J. C. Howard, J. L. Gray, A. J. Hardwick, L. T. Nguyen, and G. S. Tschumper, *J. Chem. Theory Comput.* **10**, 5426 (2014).
- [28] C. Leforestier, *J. Chem. Phys.* **140**, 074106 (2014).
- [29] The works of Leforestier *et al.* [37] and of Schenter *et al.* [39] pay considerable attention to the contribution of resonant states and long-range interactions to the canonical partition function. Such effects were found to be minimal for the temperatures of interest here and so were not considered.
- [30] A. W. Jasper, K. M. Pelzer, J. A. Miller, E. Kamarchik, L. B. Harding, and S. J. Klippenstein, *Science* **346**, 1212 (2014).
- [31] E. Miliordos, E. A. Apra, and S. S. Xantheas, *J. Chem. Phys.* **139**, 114302 (2013).
- [32] S. S. Xantheas, C. J. Burnham, and R. J. Harrison, *J. Chem. Phys.* **116**, 1493 (2002).
- [33] H.-J. Werner, P. J. Knowles, G. Knizia, F. R. Manby, M. Schütz *et al.*, MOLPRO, version 2012.1, <http://www.molpro.net>.
- [34] M. J. Frisch *et al.*, Gaussian 09, revision b.01.
- [35] J. Troe, *J. Chem. Phys.* **66**, 4745 (1977).
- [36] A. W. Jasper and J. A. Miller, *Combust. Flame* **161**, 101 (2014).
- [37] H. Sabbah, L. Biennier, S. J. Klippenstein, I. R. Sims, and B. R. Rowe, *J. Phys. Chem. Lett.* **1**, 2962 (2010).
- [38] A. K. Shukla, C. Moore, and A. J. Stace, *Chem. Phys. Lett.* **109**, 324 (1984).
- [39] Z. Shi, J. V. Ford, S. Wei, and A. W. Castleman, *J. Chem. Phys.* **99**, 8009 (1993).
- [40] P. P. Radi, P. Beaud, D. Franzke, H.-M. Frey, T. Gerber, B. Mischler, and A.-P. Tzannis, *J. Chem. Phys.* **111**, 512 (1999).
- [41] F. Dong, S. Heinbuch, J. J. Rocca, and E. R. Bernstein, *J. Chem. Phys.* **124**, 224319 (2006).
- [42] B. E. Rocher-Casterline, L. C. Ch'ng, A. K. Mollner, and H. Reisler, *J. Chem. Phys.* **134**, 211101 (2011).
- [43] C. Leforestier, K. Szalewicz, and A. van der Avoird, *J. Chem. Phys.* **137**, 014305 (2012).
- [44] A. Shank, A. Wang, B. Kaledin, B. J. Braams, and J. M. Bowman, *J. Chem. Phys.* **130**, 144314 (2009).
- [45] Y. Wang and J. M. Bowman, *J. Chem. Phys.* **135**, 131101 (2011).
- [46] L. C. Ch'ng, A. K. Samanta, Y. Wang, J. M. Bowman, and H. Reisler, *J. Phys. Chem. A* **117**, 7207 (2013).
- [47] J. A. Nelder and R. Mead, *Comput. J.* **7**, 308 (1965).